Tellus (1980), *32*, 215–231

Prediction of African waves and specification of squall lines

By T. N. KRISHNAMURTI, RICHARD J. PASCH and PHILIP ARDANUY, *Department of Meteorology, Florida State University, Tallahassee, Florida 32306, U.S.A.*

(Manuscript received August 22; in final form November 12, 1979)

ABSTRACT

This paper is part of a sequence of numerical weather prediction efforts utilizing the special observations from the GARP Atlantic Tropical Experiment (GATE). These observations, along with those available from the World Weather Watch, provide a unique opportunity to carry out numerical weather prediction (NWP) studies over portions of West Africa and the eastern Atlantic ocean utilizing high resolution limited area models. The present study reports on the results of 34 short-range numerical weather prediction experiments, with two simple models, designed to study the westward propagation of African waves. In the time frame of 24 to 48 hours, predictions at 700 mb (the level of maximum amplitude of these waves, and the level of non-divergence) show extremely promising results. These results are comparable to fine-mesh predictions in higher latitudes. Errors in phase speed and vector root mean square (RMS) wind errors are summarized for the third phase of GATE. A second part of this study deals with the problem of specification of the West African squall line with respect to the position of the predicted trough line of the African wave. A body of recent literature provides useful observational statistics relating the position of African waves, certain geographical regions, the time of day and the formation of line squall systems. These studies also provide information on the relative speeds of westward motion of the squall line and the wave trough. The decay of the squall lines during their westward propagation away from the trough is also a part of these observational statistics. Based on these observations, an empirical set of selection rules may be defined to specify the squall lines with respect to the predicted motion field. Successful results were obtained in the time frame of 24 to 48 hours for these experiments, the results of which are summarized below.

1. Introduction

A series of experiments on numerical weather prediction with the GATE data sets are presently being conducted at Florida State University. The first of the studies (Krishnamurti et al., 1979a) reported on the impact of radiative and other physical processes on African disturbances. In that study, a multilevel, fine-mesh, primitive equation model was integrated to 4 days with the data sets from two initial states. A number of experiments were carried out to investigate the impact of diurnally varying radiative (including cloud feed-back) processes on the energetics of the GATE disturbances. The principal finding of this study was a demonstration of the close coupling between the westward propagating African waves and the broad scale African monsoons on the time scale of 3 to 4 days. The role of radiative and convective processes was most crucial for the maintenance of the latter (i.e. the monsoons) which in turn were noted to be important for supplying the eddy kinetic energy for the imbedded wave disturbances. This study, furthermore, compared the performance of several different numerical weather prediction models. Among these, the single level barotropic and primitive equation models were shown to be most promising for studies on the westward propagation of African waves when these models were applied at the 700 mb level. The

 0040-2826/80/030215-17$02.50/0

choice of 700 mb for the single level NWP models appeared appropriate from the following considerations:

(i) The maximum amplitude of the African waves (v-component) is noted to occur near this level (Thompson et al., 1979).

(ii) Barotropic energy exchanges $\langle K_Z \cdot K_E \rangle$ are large at this level (a list of useful symbols appear in Table 1). In the single level models the energy exchange $\langle K_Z \cdot K_E \rangle$ describes essentially the barotropic contribution, i.e. the product of the mean zonal flow and the convergence of eddy flux of westerly momentum.

(iii) The intensity of the lower tropospheric West African jet is largest near this level. In fact, the jet core appears closer to 600 mb (Thompson et al., 1979).

(iv) The level of non-divergence appears to be close to 700 mb over the GATE- region (Thompson et al., 1979; Krishnamurti et al., 1979a).

The objectives of the present study include:

(i) *An investigation of the predictive capabilities of the single level models utilizing an increased number of experiments.* Our specific interests lie in the prediction of the position of the trough lines of the African waves and in the evolution of the motion field. The results of 34 NWP experiments are reported in the present study.

(ii) *Specification of the formation and motion of squall lines over West Africa relative to the predicted position of the trough line and the motion field.* A body of literature and recent statistics points to some interesting relationships between the position of trough lines, the motion field in the easterly waves and the evolution of West African squall lines. We shall present a short review of these observational findings and establish a set of useful criteria for the specification of squall lines from the predicted motion field. This is a non-interactive approach, where the likely region of formation and evolution of the squall line is specified without any mesoscale-synoptic scale dynamic or thermodynamic interactions. The single level models, with their conservation laws (absolute or potential vorticity), are capable of providing the background information necessary for the predictive use of these observational statistics. This is one of the goals of the following experiments.

Table 1. *List of useful symbols*

f	earth's vorticity
g	earth's gravity
h	terrain height
u	zonal wind component
v	meridional wind component
z	free surface height
k	kinetic energy
J	Jacobian operator
D/Dt	Lagrangian operator
∇^2	Laplacian operator
β	meridional deviative of the earth's vorticity
ζ	relative vorticity
ζ_p	potential vorticity
ϕ	latitude
ψ	streamfunction
$(\bar{\ })$	zonal mean
$\langle K_Z \cdot K_E \rangle$	barotropic energy conversion (zonal kinetic to eddy kinetic)
$\langle P_Z \cdot K_Z \rangle$	baroclinic energy conversion (zonal potential to zonal kinetic)
$\langle P_E \cdot K_E \rangle$	baroclinic energy conversion (eddy potential to eddy kinetic)

2. Data sources and analysis procedures

The GATE analyses in our studies includes an effort at six levels of the troposphere (Krishnamurti et al., 1979a). The motion field at 700 mb, relevant to the waves identified here, utilizes the following final validated GATE data sets:

(i) Land area World Weather Watch. This includes the radiosonde/rawinsonde network plus the pilot balloon data.

(ii) Upper wind observations from GATE ships.

(iii) Low resolution aircraft data at or around the 3 km level.

Data for only one map time, i.e. 12 GMT, were used to define the initial states for the various experiments during the third phase of GATE.

The analysis method consists of two parts:

(i) An objective analysis utilizing a successive correction method (Cressman, 1959; Tripoli and Krishnamurti, 1975) is performed on the wind observations. The off-time as well as off-level observations are incorporated via time- and space-dependent weighting functions. The first guess field is provided by a manually analyzed phase III mean map.

(ii) In relatively data-void areas, a manual analysis is made to extract subjective winds for insertion into a next cycle of the objective analysis. These subjectively analyzed vectors constitute less than 5% of the total wind observations on a given map. The analysis is displayed by a computer-drawn streamline program for further manual corrections. This is done in order to provide vertical continuity among the different analysis levels.

All of the 21 days of the third phase of GATE were analyzed by this procedure. Fig. 1 illustrates an example of the final analysis at 700 mb. This diagram illustrates an easterly wave over the GATE A/B scale ship array and an African wave. Several other examples are presented in the following sections. We believe that a high quality set of motion fields has emerged, with subjective inserts in data-sparse areas, with a reasonable space-time continuity.

3. The tropical barotropic model

A carefully designed barotropic model (Krishnamurti and Pearce, 1977) has been used for experimental NWP studies of the tropical motion field. This model utilizes the well-known quadratic conserving scheme (Arakawa, 1966) for the non-linear advective terms. This model has been tested in various applications with the GATE data sets (Krishnamurti et al., 1979a). The model conserves the absolute vorticity for parcel motions and preserves the domain averages of kinetic energy and square vorticity for periods of the order of 4 days. Examples of extremely successful 96 hour predictions over the GATE region at 700 mb were presented in Krishnamurti et al. (1979a). The basic features of the present model include:

(i) Conservation of absolute vorticity, i.e.

$$\frac{\partial}{\partial t}\nabla^2\psi = -J(\psi, \nabla^2\psi) - \beta\frac{\partial\psi}{\partial x} \quad (1)$$

(ii) Second-order Arakawa Jacobean for the advective terms.

(iii) A standard second-order Laplacian for the finite representation of ∇^2.

(iv) An Euler backward-time differencing scheme following Matsuno (1966).

(v) A fast Fourier transform method for solution of the Poisson equation for the stream-function (Hockney, 1965).

(vi) A cyclic region extends the observational region to the east over an approximate distance of 1000 km (Krishnamurti, 1969).

(vii) The initial streamfunction is defined from the initial horizontal motion field following Mathur (1970).

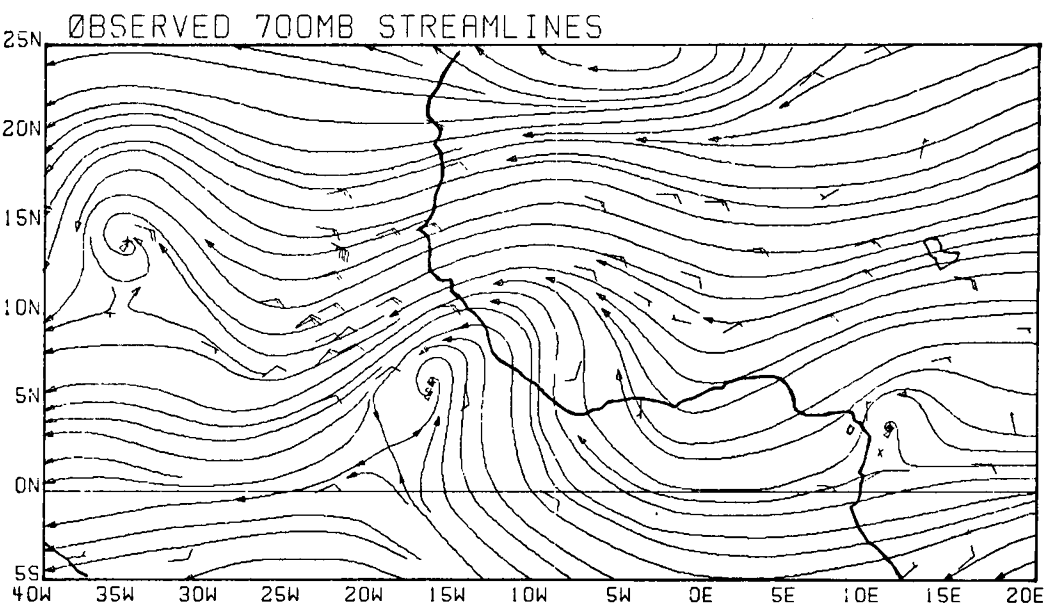

Fig. 1. Typical 700 mb data coverage and objectively analyzed streamlines: September 4, 1974, 1200 GMT.

(viii) The domain extends from 15° S to 25° N and 50° W to 10° E. The horizontal mesh size is 1° latitude/1° longitude.

(ix) The initial streamfunction ψ varies in the zonal direction at the northern and southern walls of the computational domain.

(x) The tendency of the streamfunction, $\partial\psi/\partial t$, is set to zero at the two walls during the integrations. At the zonal extremities of the computational domain, in spite of the cyclic initial state, $\partial\psi/\partial t$ is still set to zero during the integration to prevent the retrogression of domain scale waves.

(xi) The evaluation of vorticity advection at the northern and southern boundaries is carried out following Arakawa (1966).

(xii) No explicit smoothing, other than that implied within the finite differencing of the time tendency and the advective terms, is found necessary in this model.

4. One-level primitive equation model

This is the next model in line to the simple barotropic model which can be used to study the westward propagation of an African wave. It should be noted that this model has been identified by the following names: (i) Shallow water equations, (ii) Divergent barotropic model, (iii) Laplaces Tidal Equation, and (iv) one-level primitive equation model. Following our earlier papers we have designated the last name since it utilizes the undifferentiated form of the primitive equations and permits external gravity waves.

This model includes parcel invariants, such as potential vorticity $\zeta_p = (\zeta + f)/z$ and all its powers, i.e. ζ_p^n. Domain invariants of this model (for a closed domain) include: The domain averaged potential vorticity ζ_p and all its powers ζ_p^n; a total energy parameter $(gz^2/2) + kz$ and the mean height of the free surface z. In the design of this model the finite number of grid points restricts our ability to conserve only a few of the above invariants, namely the mean potential vorticity, the mean total energy and the mean height of the free surface. During the design of the finite difference analog of the one-level primitive equation model, tests were performed to verify conservation of the invariants with a closed boundary. However, in the actual prediction experiments, the meridional boundaries were subsequently left open in order to provide more realistic flows. It should be noted that the conservation of the above-stated properties does not hold for open systems. We have, however, kept track of the mean potential vorticity, mean total energy and the mean geopotential in the following open boundary integrations. These parameters were noted to vary by less than 10% of their initial values at the end of the 4-day integrations.

4.1 *The basic equations*

(i) *Equations of motion:*

$$\frac{Du}{Dt} = fv - g\frac{\partial}{\partial x}(z + h) = A \tag{2}$$

$$\frac{Dv}{Dt} = -fu - g\frac{\partial}{\partial y}(z + h) = B \tag{3}$$

$$\frac{Dz}{Dt} = -z\left(\frac{\partial u}{\partial x} + \frac{\partial v}{\partial y}\right) = C \tag{4}$$

(here)

$$\frac{D}{Dt} \equiv \frac{\partial}{\partial t} + u\frac{\partial}{\partial x} + v\frac{\partial}{\partial y} \tag{5}$$

(ii) *Semi-Lagrangian advection:* Following Krishnamurti (1969) and Mathur (1970), the above equations are numerically integrated by using the semi-Langrangian advective scheme. This requires determining the coordinates of the origin of a parcel that arrives at a grid point (i, j) in a time step Δt, following the dynamics of this model. This entails a successive correction procedure which updates the location of the origin, as well as the magnitude of forcing functions A, B and C, during each scan of the correction.

(iii) *Boundary conditions:* In the zonal direction, the domain is made cyclic by providing an artificial region initially at the eastern end of the "observational domain". This extension is carried out over a distance of roughly 1000 km. This is carried out, following Krishnamurti (1969), for the velocity components u and v initially, while the geopotential over the entire domain is determined by a solution of the reverse balance equation followed by a dynamic initialization (Kanamitsu, 1975). The southern ($\phi = \phi_S$) and the northern ($\phi = \phi_N$) boundaries are defined such that the time tendencies of u and v are set to zero, while the geopotential z is defined from the geostrophic condition $z = \bar{z} + f/g(\psi - \bar{\psi})$. Here ψ is a streamfunction which is defined following Mathur (1970), $\bar{z}$ is the mean height of a standard atmosphere at the appropriate latitudes of the two boundaries ϕ_S and ϕ_N, and $\bar{\psi}$ the zonal average of the streamfunction at these respective boundaries. In this analysis, following Mathur (1970), the conservation of mass over the domain is assured by a small correction to the outward normal flow V_n at the boundaries by the relations,

$$V_n^m = V_n + \varepsilon |V_n| \quad (6)$$

$$\varepsilon = -\int_s V_n \, ds / \int_s |V_n| \, ds \quad (7)$$

Where V_n^m is the modified outward normal velocity and the integral is carried out around the computational domain. This correction is made to the initial data and the subsequent mass conservation is assured by the vanishing of the time tendencies at the boundaries.

5. The bottom topography *h*

Fig. 2 illustrates smoothed mountains over West Africa that were used in the present series of experiments. They are extracted from the tabulations of Gates and Nelson (1975). Among these, the Guinea mountains, the Cameroons, the Tibesti and Ahaghaar are some of the prominent mountains. The treatment of these mountains in the primitive equation model is discussed in Krishnamurti et al. (1979a), where it is shown that these mountains do have a significant influence on African waves on the time scale of 2 to 4 days.

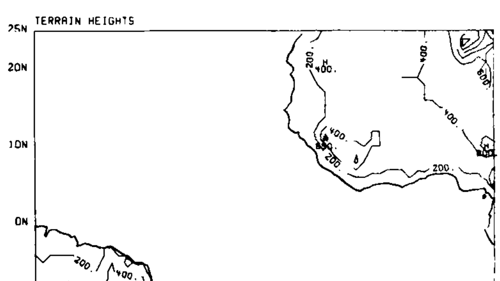

Fig. 2. Smoothed terrain heights (meters) over the West African region.

6. Mean height of the free surface

The assignment of a mean height of the free surface for the shallow water equations is important in the single level predictions. The magnitude of divergence and the phase speed of waves critically depends on the choice of this parameter. This parameter for middle latitude prediction at 500 mb is usually assigned a value 3 km, while for low latitude predictions at 700 mb one uses a value of 2 km (Krishnamurti et al., 1979a). This requires that the maximum height of mountains be roughly 50% of these values. Some smoothing of the mountain elevations is usually carried out to satisfy this constraint. Since most of the mountains over West Africa have a maximum height of roughly 1 km, no drastic smoothing, beyond that implicit in the tabulation of Gates and Nelson (1975) was necessary.

7. Prediction experiments

A total of 34 NWP experiments were carried out with the two models. Here we shall present a summary of the results and illustrations for a few examples.

Here "Model 1" refers to the barotropic model and "Model 2" refers to the simple primitive equation model. Fig. 3a, b, c and 3d, e, f respectively show one example of the 24 and 48 hour forecasts. The top panels a and d illustrate the observed fields valid at 24 and 48 hours respectively. The middle panels b and e respectively illustrate the forecasted flow fields at hours 24 and 48 from Model 1 while the panels c and f illustrate those from Model 2. Fig. 4 illustrates another example from the prediction experiments for the third phase of GATE. The illustrations show the flow fields (isotachs and streamlines) at 700 mb. The heavy dark lines indicate the trough positions for the African waves. Table 2 identifies the approximate trough positions for all the experiments (see Krishnamurti *et al.*, 1979b, for details) for the 24 and 48 hour predictions. The predicted trough positions are in close agreement with the observed positions. The errors in the trough positions are about 1° to 2° longitude for the 24 hour positions and roughly 2° to 3° longitude for the 48 hour positions. The largest forecast error in the 24 hour prediction was encountered for

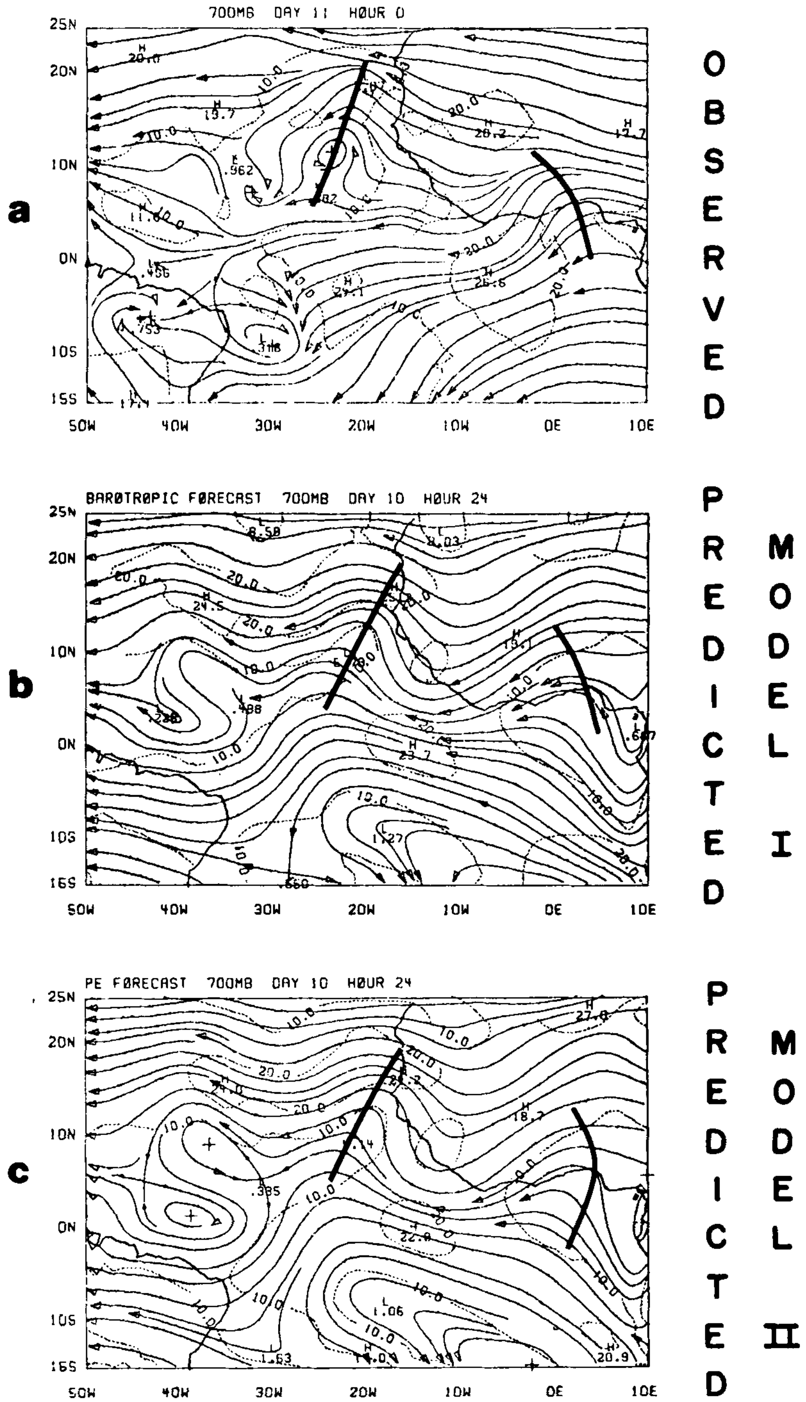

Fig. 3. The observed and predicted motion field of 700 mb (light solid lines, streamlines; dashed lines, isotachs in knots; heavy solid lines, trough axes). For hours 24 and 48: (a) observed motion field valid at 1200 GMT, September 9, 1974, (b) 24 hour barotropic forecast verifying at 1200 GMT, September 9, 1974, (c) 24 hour one-level primitive equation forecast verifying at 1200 GMT, September 9, 1974.

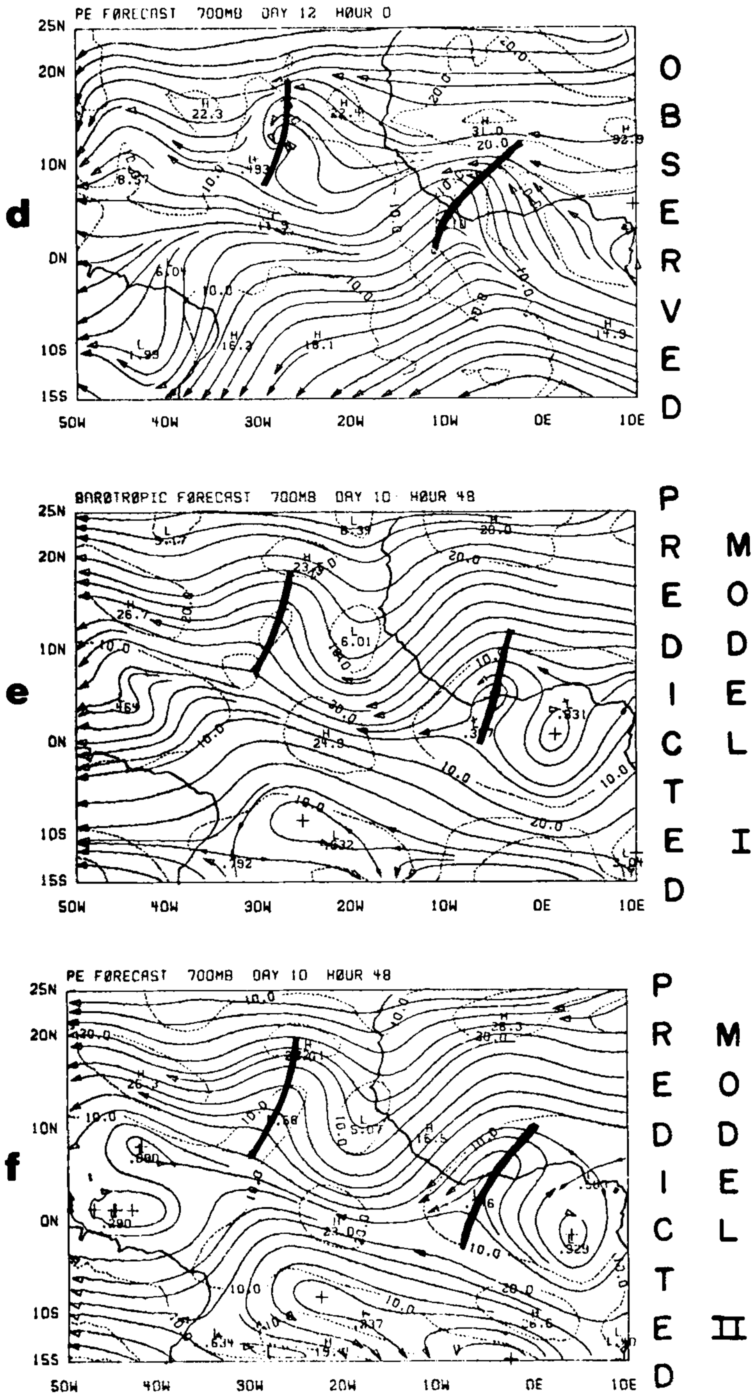

Fig. 3 (*cont.*). (d) Observed motion field valid at 1200 GMT, September 10, 1974, (e) 48 hour barotropic forecast verifying at 1200 GMT, September 10, 1974, (f) 48 hour one-level primitive equation forecast verifying at 1200 GMT, September 10, 1974.

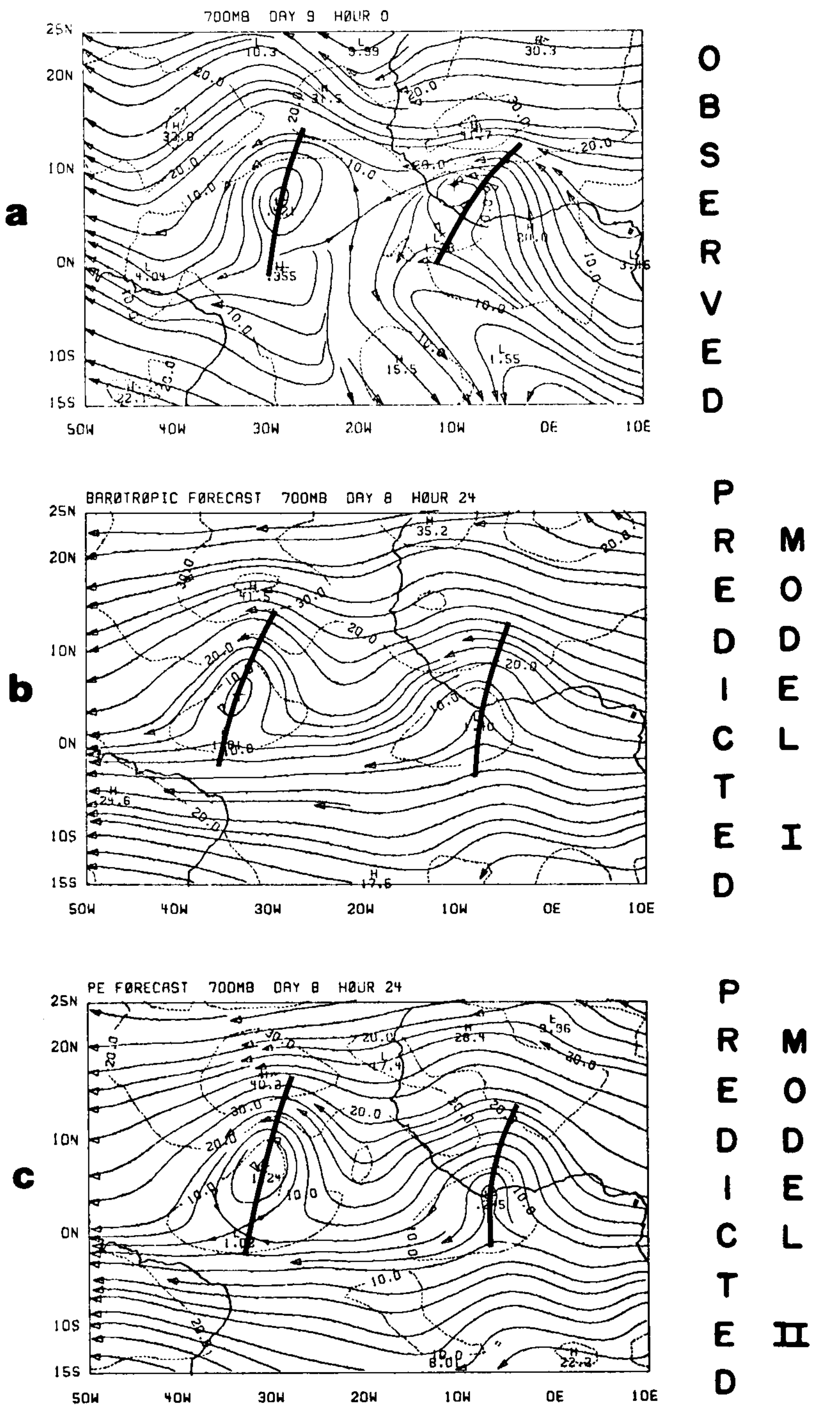

Fig. 4. The observed and predicted motion field of 700 mb (light solid lines, streamlines; dashed lines, isotachs in knots; heavy solid lines, trough axes). For hours 24 and 48: (a) observed motion field valid at 1200 GMT, September 7, 1974, (b) 24 hour barotropic forecast verifying at 1200 GMT, September 7, 1974, (c) 24 hour one-level primitive equation forecast verifying at 1200 GMT, September 7, 1974.

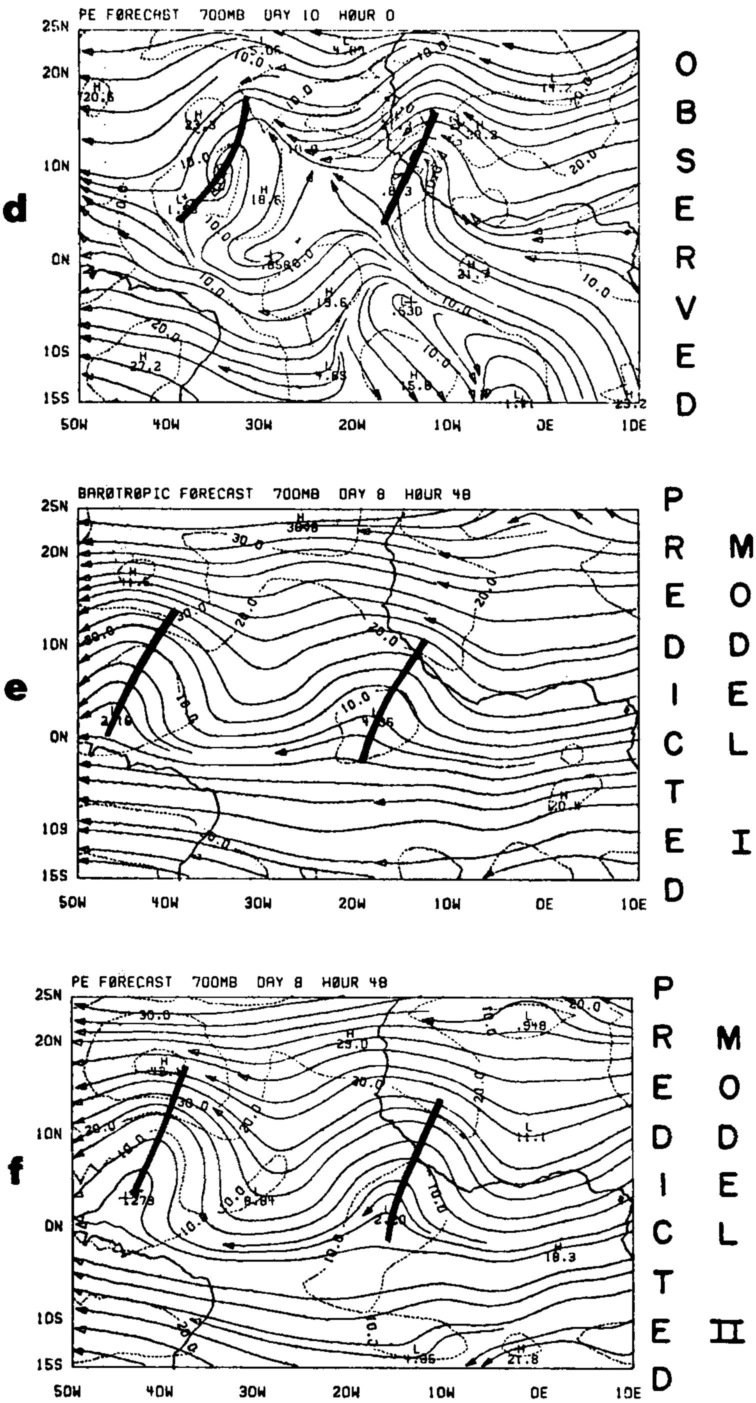

Fig. 4 (cont.). (d) Observed motion field valid at 1200 GMT, September 8, 1974, (e) 48 hour barotropic forecast verifying at 1200 GMT, September 8, 1974, (f) 48 hour one-level primitive equation forecast verifying at 1200 GMT, September 8, 1974.

Table 2. *Approximate trough positions for the experiments illustrated here*

Time of initial state	Wave No.	Approximate mean longitudinal position of trough: 24 hours Observed	24 hours Model I	24 hours Model II	48 hours Observed	48 hours Model I	48 hours Model II
Sept. 13, 1974 12Z	1	8 W	6 W	5.5 W	12 W	12 W	11 W
	2	30 W	32 W	30 W	35 W	36 W	35 W
Sept. 10, 1974 12Z	1	12 W	12 W	13 W	18 W	19 W	20 W
	2	39 W	35 W	34 W	Moved out of domain		
Sept. 8, 1974 12Z	1	0°	0°	1° W	8 W	7 W	5 W
	2	24 W	22 W	22 W	29 W	30 W	29 W
Sept. 7, 1974 12Z	1	11 W	11 W	12 W	22 W	22 W	21 W
	2	35 N	39 W	39 W	Moved out of domain		
Sept. 6, 1974 12Z	1	9 W	9 W	9 W	12 W	16 W	14 W
	2	28 W	32 W	31 W	32 W	41 W	40 W
Sept. 4, 1974 12Z	1	2 E	3 E	2 E	9 W	10 W	10 W
	2	20 W	21 W	22 W	26 W	30 W	31 W
Sept. 1, 1974 12Z	1	20 W	22 W	23 W	27 W	27 W	27 W
	2	39 W	39 W	39 W	Moved out of domain		
Aug. 30, 1974 12Z	1	3 W	1 W	2 W	12 W	7 W	8 W
	2	28 W	27 W	27 W	33 W	32 W	32 W

September 10 when a wave was located in a relatively data-sparse area around 39°W longitude where the verification charts were, in fact, questionable. The single level predictions of both models (the non-divergent and the divergent) have comparable accuracy; this is perhaps related to the fact that the level of non-divergence over the GATE region is around 700 mb (Thompson et al., 1979; Krishnamurti *et al.*, 1979a).

The flow fields (i.e. direction and speed) show that, overall, the predictions at 24 and 48 hours are in reasonable agreement with observations.

One measure of the accuracy of the forecasts is root mean square (RMS) vector deviation of the forecast model relative to the verification winds. This was computed at hours 24 and 48 over an inner domain bounded by the latitudes 0° and 15° N and the longitudes 0° and 25° W. Fig. 5 depicts the magnitude of this quantity, averaged over all verifiable forecasts (RMSF). It increases from 5.15 m s^{-1} at hour 24 to 6.20 m s^{-1} at hour 48. Persistence may also be used as a comparable measure of prediction. The mean RMS vector deviation of the persistence winds relative to the verification winds (RMSP) is computed for hours 24 and 48. The error increases from 6.98 m s^{-1} at hour 24 to 8.41 m s^{-1} at hour 48. In both cases the forecast error is significantly lower, indicating that NWP of the wind field at 24 and 48 hours are better than persistence. In the tropics, climatology is often useful where data are unavailable. Computation of the RMS vector deviation of the time mean winds relative to the verification winds (RMSC) gives a value of 6.87 m s^{-1}. Thus, at 24 hours, the forecast winds are significantly more accurate than either persistence or climatology.

The prediction experiments in general exhibited a decay of the maximum wind in the belt of the strong easterlies around 15° N shown in Table 3.

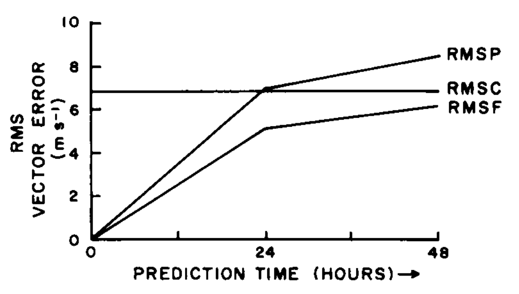

Fig. 5. Magnitude of the RMS vector deviation of the model II forecast winds relative to the verification winds (RMSF); magnitude of the RMS vector deviation of the persistence winds relative to the verification winds (RMSP); magnitude of the RMS vector deviation of the phase III climatology winds relative to the verification winds (RMSC). The three curves are the averages over all verifiable forecasts.

Table 3. *Maximum speed of the easterlies (knots) near 15° N (east of 30° W)*

Time of initial state	At 24 hours			At 48 hours		
	Observed	Model I	Model II	Observed	Model I	Model II
Sept. 13, 1974 12Z	32	25	26	33	27	25
Sept. 10, 1974 12Z	26	20	22	39	22	31
Sept. 8, 1974 12Z	20	25	24	31	23	21
Sept. 7, 1974 12Z	28	28	30	20	26	27
Sept. 6, 1974 12Z	42	30	28	28	21	23
Sept. 4, 1974 12Z	36	32	35	41	30	32
Sept. 1, 1974 12Z	32	28	24	38	21	21
Aug. 30, 1974 12Z	33	24	24	34	20	20

The decay is evidently related to model initialization and the restrictions on the boundary values of u, v and z. The prediction experiments also exhibited a tendency to carry an easterly velocity maximum westward along with the easterly wave at its poleward edge. The observations, although not sufficient, did not always seem to bear this out. The kinetic energy, following a parcel, is not an invariant for these models. Hence the maximum speed is not expected to retain its magnitude in these one-level integrations. The domain averaged kinetic energy (or total energy) is noted to remain nearly constant (within 10% of the initial values). Our results show a decrease of velocity in the high speed regions and an increase in the low speed regions. This is, most likely, due to nonbarotropic effects, subgrid scale processes and the computational smoothing inherent in the finite differencing of the forcing functions A, B and C as well as the smoothing due to the finite representation of the semi-Lagrangian advection. In order to improve the low latitude NWP efforts in this direction systematic extensions of present work are desirable with multilevel grid point and spectral models. The latter are better suited since they avoid the space truncation and related smoothing. Only a few experiments have been made thus far with multilevel grid point models (Krishnamurti et al., 1979a), and these seem to describe the eddy kinetic energy of African waves somewhat better than the single level formulations shown here. Since the present study focuses on the capabilities of the one-level model, i.e. in its description of the trough location, and in the specification of the relative location of a squall line, we feel that the above limitations are not critical during the first 48 hours.

8. The specification of squall lines

An important phenomenon which is often associated with African waves is the West African Disturbance Line or squall line. It has been described by Hamilton and Archibold (1945) and Eldridge (1957). In a recent study, Payne and McGarry (1977) noted that, during Phase III of GATE, squall lines were most frequently initiated ahead of the wave trough, near to the region of maximum northerly winds at 700 mb. They furthermore noted that these squall lines move westward at an average speed of roughly 16 m s^{-1}, about twice the phase speed of the wave, and decayed in the vicinity of the downstream ridge. Moreover, they indicated a mean lifetime of around 10 hours and a mean latitude of about 13° N for the squall lines.

Much of the intense rainfall over West Africa occurs in association with squall lines (Cocheme and Franquin, 1967). The following aspects of the diurnal change in the heavy precipitation are of interest here. McGarry and Reed (1978) note that:

(i) Over West Africa, around 15° to 20° N, the rain amounts are greatest just prior to midnight.
(ii) Over the Eastern Atlantic, in the vicinity of the GATE ship array, the rainfall maximum occurs in the early afternoon hours (1400 local time).
(iii) Over West Africa, south of 15° N, the diurnal amplitudes are much smaller, but it appears likely that the rainfall maximum occurs in the late afternoon or early evening.

The general character of the diurnal variation of heavy precipitation over West Africa noted by

McGarry and Reed (1978) suggests that the squall lines are in their mature stage during the early evening hours. Thus, it seems reasonable to assume that most of the squalls were initiated during the late afternoon. This is confirmed by the findings of Martin (1975) which indicate a preferred time of development for the squalls of around 1800 GMT (within an hour of local time for most parts of West Africa).

Aspliden et al. (1976) investigated squall line occurrences during the three phases of GATE and found that they tended to form in preferred geographic regions over West Africa. Their data indicate that there exists a maximum in the frequency of squall line generation between 0° and 10° W longitude with a secondary maximum of generation frequency between 5° and 10° E longitude. Moreover, they state that nearly all of the lines were confined within the latitudes of 7° and 17° N, with the squalls typically propagating westward at around 60 km h^{-1}. These findings are in general agreement with the previously quoted results of Payne and McGarry.

From the statistics compiled by the aforementioned researchers and the results of our numerical prediction experiments, a simple empirical procedure has been developed for the specification of the formation and subsequent motion of West African squall lines:

(i) Each of the seventeen 30 hour[1] 700 mb primitive equation forecasts verifying at 1800 GMT are inspected to see if the longitude of maximum northerly winds ahead of the wave trough lies in the zone extending from 0° to 10° W longitude. If this criterion is not met, it is assumed a squall line will not form.

(ii) If criterion (i) is satisfied, squall line formation is specified at this longitude, with a latitudinal extent from 7° to 17° N.

(iii) The specified squall line is assumed to move westward at twice the predicted wave phase speed, which is determined from the predicted trough positions between hours 30 and 39.

(iv) The squall line is assumed to dissipate 10 hours after formation.

We applied the above procedure to the numerical forecasts and noted that 8 of the 17 days considered met the above selection rules. Two examples of the forecasted 700 mb fields and evolution of the specified squall lines (dashed lines) are shown in the left panels of Figs. 6a and 6b. On the right panels of Figs. 6a and 6b are the cloud photographs from the infrared imagery of the SMS-1 satellite. On these photographs we have superimposed dashed lines over those cloud clusters which were associated with squall lines within the belt from 0° to 10° W longitude. Here we have employed essentially the same criteria to identify a squall line cluster as used by Payne and McGarry (1977), i.e. explosive growth, high brightness and a fairly distinct leading edge. It should be noted here that we have marked the approximate center of the squall line clusters for clarity. However, for verification purposes the leading edge of the cluster's cirrus shield, which was found by Aspliden et al. (1976) to coincide with the heaviest rainfall, has been used to denote the observed position of the squall line for this study. A squall line was observed on each of the eight days and in one of the cases (12 September) two were observed, albeit one of these (a cluster near 4° W longitude at 1800 GMT) just barely qualifies as a squall line. As can be seen from the satellite pictures in Figs. 6a and 6b and others illustrated in Krishnamurti et al. (1979b), all of the observed squall lines are near their formative stages at hour 30 (1800 GMT), and near their dissipative stages at hour 39 (0300 GMT on the next day). This is consistent with the previously stated notion of formation at around 1800 GMT and dissipation roughly 10 hours later that was used to develop the specification procedure.

The results of the squall line specification experiments are summarized in Table 4. The mean

[1] We could have selected either the 6 or 30 hour forecast for this purpose, but it is obvious that using the 30 hour forecast strengthens the predictive value of this technique.

Fig. 6. Left panel: predicted 700 mb streamlines and isotachs (one-level primitive equation model) for hours 30 (top) to 39 (bottom) at time intervals of 3 hours. Verification times are 1800 GMT to 0300 GMT the following day. The specified (via NWP model) squall lines are indicated by heavy dashed lines. Right panel: Corresponding satellite photographs with an observed squall line in the belt from 0° to 10° W longitude indicated by heavy dashed lines. (a) Verifying September 2/September 3. (b) Verifying September 6/September 7.

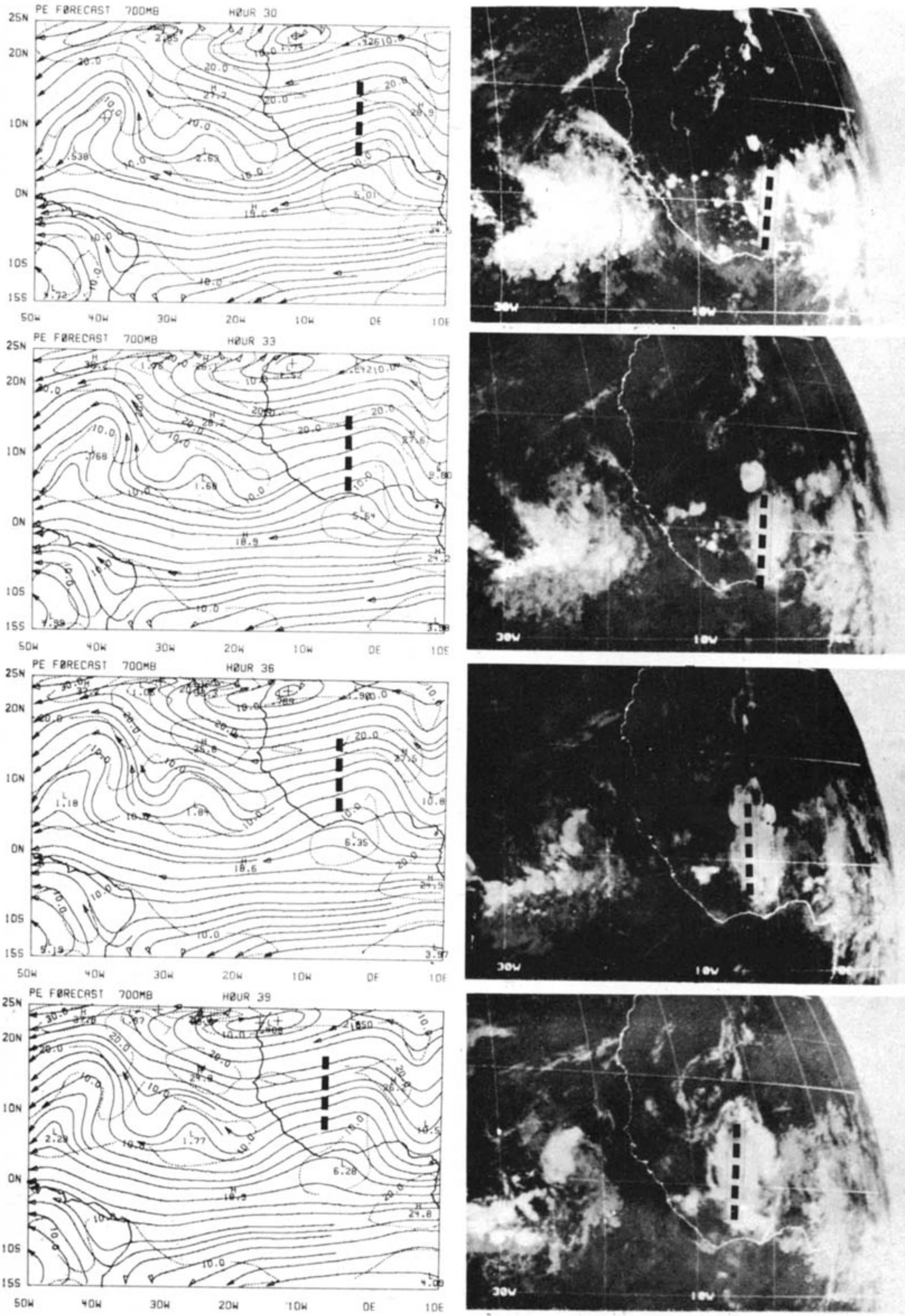
PE FØRECAST 700MB HØUR 30
PE FØRECAST 700MB HØUR 33
PE FØRECAST 700MB HØUR 36
PE FØRECAST 700MB HØUR 39
25N
20N
10N
0N
10S
15S
50W
40W
30W
20W
10W
0E
10E
30W
10W

6a

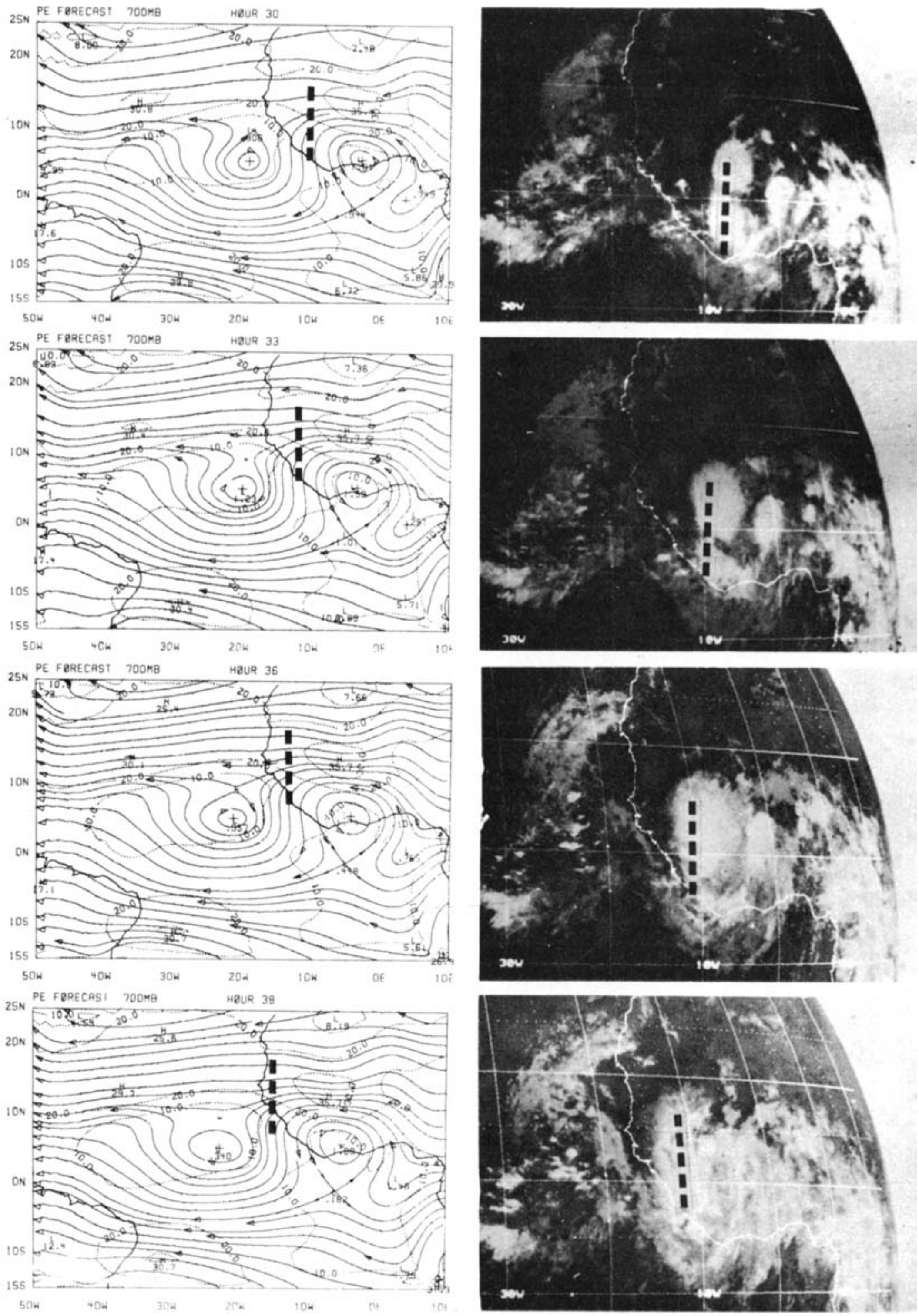
PE FØRECAST 700MB HØUR 30
PE FØRECAST 700MB HØUR 33
PE FØRECAST 700MB HØUR 36
PE FØRECAST 700MB HØUR 39
25N
20N
10N
0N
10S
15S
50W 40W 30W 20W 10W 0E 10E
30W
10W

displacement errors for all cases at 30 and 39 hours are 2.125 and 1.625 degrees longitude respectively. The relatively large displacement errors for cases 1, 3 and 4 are ascribed mainly to deficiencies in the numerical forecasts of trough phase speed and tilt. Further details on the individual squall line episodes are reported elsewhere (Krishnamurti et al., 1979b).

9. Concluding remarks

Not many tests on the performance of NWP models over low latitudes, with large samples of experiments, have been undertaken. Vanderman and Collins (1967) and Ramanathan (1976) have published the results of operational NWP efforts. The data coverage for operational NWP efforts is known to be very poor. The present series of 34 experiments summarized in this paper utilizes the final validated GATE data sets and provides a better coverage than has been possible in the past in the low latitudes. The series of experiments reported in this paper deal with the performance of a barotropic and a simple primitive equation model in low latitudes. When these models are applied at the 700 mb level, we notice that, on the average, phase errors total on the order of 1.6° longitude after the first 24 hours and 2.1° longitude after the full 48 hours. The magnitudes of the vector wind errors in the 24 and 48 hour periods are of the order of 6 m s^{-1} respectively. The two models, in general, do not show any appreciable differences in their predictions; however, for certain cases the influence of the west African mountains is large and Model II (with bottom topography) is noted to perform better than Model I (Krishnamurti et al., 1979a). The energetics of the model was also determined during the course of integration for each of the experiments. The barotropic energy exchange has a natural tendency to change sign, from whatever it is initially, in the course of 3 to 5 days in these models. We believe that it is an undesirable aspect of the barotropic models since the sign of the barotropic energy exchange can, in principle, maintain the same sign if other forms of energy exchange permit it to do so. For example, local Hadley type overturnings can maintain an exchange, $\langle P_Z \cdot K_Z \rangle > 0$, and thus provide a steady supply of energy to the zonal kinetic energy, which in turn could supply energy, $\langle K_Z \cdot K_E \rangle > 0$, to the waves steadily. In view of this model bias in the energy exchange, we feel that the barotropic model energetics are only reliable during roughly one-half of the period of this oscillation, i.e. roughly 2 days. In this time frame of 1 to 2 days, we have demonstrated that the forecasts are, in fact, quite reasonable at 700 mb in this region. In this context, it is also worth noting that the initial sign of the energy exchange, $\langle K_Z \cdot K_E \rangle$, is not always positive, as is suggested for individual and composite African waves by Pedgley and Krishnamurti (1976) and Reed et al. (1977). The reason for this becomes clearer when one examines the many initial states during the phase III of GATE. We find that although a majority of waves have a southwest to northeast tilt, however, in about one-third of the cases (roughly 10 waves) the opposite tilt is also present initially. Lacking other

Table 4. *Specified (via NWP model) and observed squall line statistics. 30 hours refers to squall location at 1800 GMT on the date shown and 39 hours to location at 0300 GMT the following day*

Case	Date	30 hours (specified)	30 hours (observed)	Displacement error at 30 hours (degrees longitude)	39 hours (specified)	39 hours (observed)	Displacement error at 39 hours (degrees longitude)
1	August 31, 1974	10.0° W	13.0° W	3.0	14.0° W	19.0° W	5.0
2	September 2, 1974	2.0° W	2.0° W	0.0	8.0° W	8.0° W	0.0
3	September 3, 1974	7.0° W	12.0° W	5.0	16.0° W	16.0° W	0.0
4	September 4, 1974	0.0° W	5.0° W	5.0	7.0° W	10.0° W	3.0
5	September 6, 1974	10.0° W	9.0° W	1.0	15.0° W	14.0° W	1.0
6	September 9, 1974	6.5° W	6.0° W	0.5	12.5° W	11.0° W	1.5
7	September 12, 1974	3.0° W	4.0° W	1.0	9.0° W	8.0° W	
			10.0° W			15.0° W	1.0
8	September 13, 1974	9.5° W	8.0° W	1.5	14.5° W	13.0° W	1.5

sources of energy supply in the barotropic model, some of these waves were noted to decay in the first 48 hours due to an energy exchange from the waves to the zonal flow. We believe that some of the poor forecasts, illustrated here, lack the transfer of energy via vertical mass exchanges, $\langle P_E \cdot K_E \rangle$. This is only possible within the context of multi-level primitive equation models with more complete physics (Krishnamurti et al., 1979a). Two such models (one a fine mesh grid point model and another a global spectral model) are currently being used in experimental prediction for a larger sample of experiments. The results of these will be reported later.

The specification of the squall line was an after-thought. The quality of success in the prediction of the wave trough positions in the 24 to 48 hour time frame prompted us to inquire about this predictive possibility. Observational statistics by Payne and McGarry (1977), and others, show that during the late afternoon hours, if a certain region over West Africa experiences northerly flow due to the approach of an African wave, then squall lines are quite likely to form. Our predicted positions (and time of arrival) of the wave trough in this region show reasonable skill in the specification of the formation of the squall line. The examples of squall line specification, shown here and in Krishnamurti et al. (1979b), are those that met the selection rules we prescribed for the formation of the squall lines. 30 to 39 hours after initial time in these experiments, a mean displacement error of about 2° longitude in the location of the squall line was noted. This is close to the limit of attainable accuracy for an NWP model with a mesh size of 1° longitude. The reasons for the formation remain obscure and do suggest a need for further studies on the interactions of the waves with the underlying surface and the eventual organization of the line convection, as shown in the many satellite photographs. The reasons for the faster westward motion of the squall line (roughly twice the speed of motion of the wave) as well as the decay of the squall line during its approach towards the ridge line of the African wave are beyond the scope of this study.

10. Acknowledgements

The research reported here is supported by the Climate Dynamics Section of the National Science Foundation NSF Grant No. ATM-7819363. Computational support was provided by the National Center for Atmospheric Research also supported by the National Science Foundation.

REFERENCES

Arakawa, A. 1966. Computational design for long term numerical integration of the equations of atmospheric motion. *J. Comp. Phys. 1*, 119–143.

Aspliden, C. I., Tourre, Y. and Subine, J. B. 1976. Some climatological aspects of West African squall lines during GATE. *Mon. Wea. Rev. 104*, 1029–1035.

Cocheme, J. and Franquin, R. 1967. An agroclimatology survey of a semi-arid area in Africa south of the Sahara. WMO Tech. Note No. 86, 136 pp.

Cressman, G. P. 1959. An operational objective analysis system. *Mon. Wea. Rev. 87*, 367–374.

Eldridge, R. H. 1957. A synoptic study of West African disturbance lines. *Quart. J. Roy. Met. Soc. 83*, 303–314.

Gates, W. L. and Nelson, A. B. 1975. A new (revised) tabulation of the Scripps topography on a 1° global grid. Part 1. Terrain heights. Rept. No. R-1276-1-ARPA-Rand Corporation, Santa Monica, California.

Hamilton, R. A. and Archibald, J. W. 1945. Meteorology of Nigeria and adjacent territories. *Quart. J. Roy. Met. Soc. 71*, 231–264.

Hockney, R. W. 1965. A fast direct solution of Poisson's equation using Fourier analysis. *J. Assoc. Comput. Mach. 12*, 95–113.

Kanamitsu, M. 1975. On numerical prediction over a global tropical belt. Rept. No. 75–1, Department of Meteorology, Florida State University, Tallahassee, Florida 32306. 282 pp.

Krishnamurti, T. N. 1969. An experiment in numerical prediction in equatorial latitudes. *Quart. J. Roy. Met. Soc. 95*, 594–620.

Krishnamurti, T. N. and Pearce R. P. 1977. The fundamentals of numerical weather prediction and the filtered barotropic model. Proceedings of WMO seminar, Dakar, November, 1976. WMO Rept. No. 492. Geneva, Switzerland.

Krishnamurti, T. N., Pan, H. L., Chang, C. B., Ploshay, J., Walker, D. and Oodally, A. W. 1979a. Numerical weather prediction for GATE. To appear in the October issue of the *Quart. J. Roy. Met. Soc.*

Krishnamurti, T. N., Pasch, R. J. and Ardanuy, P. 1979b. Prediction of African waves and specification of squall lines. Rept. No. 79-2, Dept. of Meteorology, Florida State U., Tallahassee, Florida 32306. 55 pp.

Martin, D. W. 1975. Characteristics of West African and Atlantic cloud clusters based on satellite data. GATE Rept. No. 14, Preliminary scientific results of the GARP Atlantic Tropical Experiment, Vol. I., 182–190.

Mathur, M. B. 1970. A note on an improved quasi-Lagrangian advective scheme for primitive equations. *Mon. Wea. Rev. 98*, 214–219.

Matsuno, T. 1966. Numerical integration of primitive equations by a simulated backward difference method. *J. Met. Soc. Japan 44*, 76–84.

McGarry, M. M. and Reed, R. J. 1978. Diurnal variations in convective activity and precipitation during phases II and III of GATE. *Mon. Wea. Rev. 106*, 101–113.

Payne, S. W. and McGarry, M. M. 1977. The relationship of satellite infrared convective activity to easterly waves over West Africa and the adjacent ocean during phase III of GATE. *Mon. Wea. Rev. 105*, 413–420.

Pedgley, D. E. and Krishnamurti, T. N. 1976. Structure and behavior of a monsoon cyclone over West Africa. *Mon. Wea. Rev. 104*, 149–167.

Ramanathan, Y. and Bansal, R. K. 1976. The NHAC operational quasi-geostrophic model. IMD Scientific Rept. No. 76/1. pp. 1–12. India Meterological Department, Lodi Road, New Delhi, India.

Reed, R. J., Norquist, D. C. and Recker, E. E. 1977. The structure and properties of African wave disturbances as observed during phase III of GATE. *Mon. Wea. Rev. 105*, 317–333.

Thompson, R. M., Payne, S. W., Recker, E. E. and Reed, R. J. 1979. Structure and properties of synoptic-scale wave disturbances in the intertropical convergence zone of the Eastern Atlantic. *J. Atmos. Sci. 36*, 53–72.

Tripoli, G. and Krishnamurti, T. N. 1975. Low level flows over the GATE area during summer 1972. *Mon. Wea. Rev. 103*, 197–216.

Vanderman, L. W. and Collins, W. G. 1967. Operational experimental numerical forecasting for the tropics. *Mon. Wea. Rev. 95*, 950–953.

ПРОГНОЗ АФРИКАНСКИХ ВОЛН И ОПРЕДЕЛЕНИЕ ЛИНИЙ ШКВАЛОВ

Статья является частью последовательности экспериментов по численному предсказанию погоды с использованием специальных наблюдений, полученных во время Атлантического тропического эксперимента ПИГАП (АТЭП). Эти наблюдения вместе с данными Службы мировой погоды обеспечивают уникальную возможность для исследований по численному предсказанию погоды над частью Западной Африки и востоком Атлантического океана с использованием модели прогноза по ограниченной территории с высоким разрешением. Настоящее исследование основано на результатах 34 экспериментов по численному краткосрочному прогнозу погоды с помощью двух простых моделей, созданных для изучения распространения Африканских волн на запад.

Прогнозы на уровне 700 мбар с заблаговременностью 24–48 часов (бездивергентный уровенъ) где эти волны достигают максимальной амплитуды-, обнаружили многообещающие результаты. Результаты сравнимы с прогнозами по учащенной сетке в более высоких широтах. Для третьей стадии АТЭП приводятся ошибки фазовой скорости и средние квадратичные ошибки определения вектора ветра. Вторая часть исследования рассматривает задачу определения Западноафриканской линии шквала по отношению к предсказанному положению ложбинной линии Африканской волны. Во многих недавних работах приводится полезная статистика данных наблюдений, связывающих за положение Африканских волн, определенные географические области, время суток с образованием линии шквалов. Эти исследования также дают информацию об относительной скорости движения на запад линии шквалов и ложбины волны. Ослабление линии шквалов по мере ее продвижения на запад по отношению к ложбине также содержится в этой статистике наблюдений. Основываясь на этих наблюдениях, можно вывести ряд эмпирических правил для определения положения линии шквалов по отношению к предсказанному полю скорости. В этих экспериментах были получены успешные результаты для прогнозов с заблаговременностью 24–48 часов. Результаты экспериментов приводятся ниже.